CAPSULE-LIKE SMART AGGREGATE-BASED CONCRETE STRESS MONITORING VIA IMPEDANCE SIGNALS: NUMERICAL STUDY

Pham Quang Quang[1]*, Huynh Thanh Canh[2], Dang Ngoc Loi[3]

[1]Danang Architecture University, Da Nang, Vietnam
[2]Duy Tan University, Da Nang, Vietnam
[3]Mien Tay Construction University, Vinh Long, Vietnam

*Corresponding author: quangpq@dau.edu.vn

(Received: April 23, 2025; Revised: June 15, 2025; Accepted: June 20, 2025)

DOI: 10.31130/ud-jst.2025.23(10C).663E

Abstract - This study numerically explores the feasibility of a capsule-like smart aggregate (CSA) for monitoring stress in concrete using an impedance-based approach. After a brief introduction to the core principles of impedance-based structural health monitoring (SHM), a finite element model of a concrete cylinder embedded with a CSA sensor is developed. Impedance responses are analyzed under varying levels of axial compressive stress. Variations in the CSA's impedance response due to applied stresses are analyzed through shifts in the frequency and amplitude of resonant peaks and quantified using the Root Mean Square Deviation (RMSD) index. The results demonstrate that the CSA sensor exhibits clear sensitivity to compressive stress changes, confirming its feasibility for stress monitoring in concrete structures.

Key words - Smart aggregate; capsule-like; PZT sensor; impedance-based; compressive stress

1. Introduction

Concrete structures (bridges, buildings, dams, and tunnels) often have an inhomogeneous property, and are frequently subjected to a significant number of external factors during service life, such as temperature, humidity, erosion, and loading [1]. The structures have to bear severe conditions such as earthquakes, tsunamis, or hurricanes. These factors could be coupled with construction uncertainties, leading to initial structural deterioration. Therefore, early monitoring of the health of concrete structures is critical to ensuring their safety and long-term integrity while also improving the efficiency of maintenance efforts.

Structural health monitoring (SHM) for concrete structures is a significant concern of many researchers and engineers [2-4]. Over the past decades, numerous global and local monitoring techniques have been developed and employed for the detection of structural damage in concrete elements [5-7]. Along with the development of monitoring methods, sensor technologies have also evolved to monitor the health of concrete structures [3].

Among local damage monitoring methods, impedance-based SHM has emerged as a promising approach [8-12]. The theoretical foundation for this method was initially developed by Liang et al. [13], and has since been extended by numerous researchers [14-17]. A key feature of the technique is the coupling interaction between a piezoelectric sensor (typically lead zirconate titanate, PZT) and the monitored structure, enabling the acquisition of electromechanical impedance responses. These responses typically span high-frequency ranges, making them highly sensitive to structural changes. Variations in the impedance signatures before and after damage events are analyzed to detect early-stage deterioration in critical structural components. Based on this principle, the method has been widely applied to identify various types of damage, such as cracking, loose connections, corrosion, and loss of prestress force, in diverse structural systems [18-21].

To enable impedance-based health monitoring of concrete structures, the PZT sensors have been installed on the target structures in various ways. Generally, these installation approaches were categorized into two main groups: surface-bonded PZT sensors [22-26] and embedded PZT sensors [27-29]. Among the latest developments in embedded sensing, the capsule-like smart aggregate (CSA) sensor [30] has emerged as a promising solution. The CSA is designed to retain the advantages of traditional embedded sensors (i.e., coated PZT, smart aggregates (SAs), and spherical SAs), which include sensor protection and the ability to monitor internal damage within concrete [27]. In addition, the CSA addresses a key limitation of conventional SAs, which often rely on a trial-and-error approach to identify sensitive frequency ranges [31]. Unlike these earlier methods, the CSA operates within a predefined frequency range below 100 kHz, enabled by a specially designed vibrating interface [30, 32]. This makes it particularly suitable for wireless impedance measurements [9, 33]. Similar to other embedded sensors, CSA sensors are typically installed in critical regions of the structure, such as load paths and areas prone to stress concentration, rather than being uniformly distributed throughout the monitored structures. While CSA sensors provide localized impedance-based measurements, their effectiveness can be enhanced by combining them with other types of sensors (e.g., accelerometers) to enable a more comprehensive assessment of overall structural behavior [34].

Laboratory-scale experiments have been conducted to evaluate the practicality and effectiveness of the CSA sensor for monitoring compressive stress in concrete cylinders [30, 35]. However, to date, no numerical studies have been reported on CSA-based compressive stress monitoring. Such studies are essential to further explore the CSA's potential for impedance-based sensing. A validated

finite element (FE) model can be developed and later updated using experimental results [35], enabling more comprehensive damage analysis, including stress variation and crack detection. Moreover, the updated model can facilitate the generation of large datasets for integration with deep learning models (e.g., CNN-based models), ultimately improving the accuracy of concrete damage monitoring [35, 36].

This study numerically explores the feasibility of using a CSA sensor for impedance-based stress monitoring in concrete structures. A brief overview of the underlying principles of impedance-based SHM is provided. A FE model is constructed to simulate a concrete cylinder embedded with a CSA sensor subjected to varying levels of axial compressive stress. The sensor's responses are analyzed by examining shifts in the resonant frequency and amplitude of the impedance spectrum, and quantified using the Root Mean Square Deviation (RMSD) index. The findings confirm that the CSA sensor is capable of detecting stress-induced changes, highlighting its potential as an effective tool for localized stress monitoring in concrete structures.

2. Fundamentals of impedance-based method

2.1. Basic theory of impedance-based SHM

Liang et al. [13] developed the concept of electromechanical impedance (EMI) using a piezoelectric-actuator mechanical system. Figure 1 shows this concept. A PZT patch is attached to the surface of a structure to acquire EMI signals from the coupling interaction between the PZT and the structure. As illustrated in Figure 1a, an applied harmonic voltage $V(\omega)$ induces a mechanical strain represented by a force $F(\omega)$ on the PZT through an inverse piezoelectric effect. The force $F(\omega)$ is assigned to the local area of the host structure. Instantaneously, the structural response is transferred back to the PZT, generating a corresponding voltage signal through a direct piezoelectric effect. This electromechanical coupling between the PZT and the structure can be represented by a one-degree-of-freedom (1-DOF) impedance model [37], as illustrated in Figure 1b. The resulting EMI response is characterized by the ratio of the input harmonic voltage $V(\omega)$ to the output electric current $I(\omega)$, and is expressed as follows:

$$Z(\omega) = \frac{V(\omega)}{I(\omega)} = \left\{ i\omega A_{pzt} \left[\hat{\varepsilon}_{33}^{T} - \frac{1}{Z_{pzt}(\omega)/Z_s(\omega)+1} d_{31}^{2} \hat{Y}_{11}^{E} \right] \right\}^{-1} \quad (1)$$

where i is the imaginary unit; ω denotes the excitation frequency; A_{pzt} is the PZT's geometric constant; $\hat{\varepsilon}_{33}^{T}$ is the complex dielectric constant at zero stress; d_{31}^{2} is the piezoelectric constant in 1-direction at zero stress; $\hat{Y}_{11}^{E}$ is the complex Young's modulus of the PZT at zero electric field; $Z_{pzt}(\omega)$ and $Z_s(\omega)$ are the structural mechanical (SM) impedances of the PZT patch and the host structure, respectively.

Since the SM impedance of the host structure is a function of its physical properties (i.e., stiffness k, mass m, and damping c), any damage-induced changes in these properties result in corresponding variations in the impedance signals. In this context, the SM impedance of the PZT patch is typically assumed to remain constant. The structural damage can therefore be detected by comparing the post-damage impedance response to the baseline (pristine) signal.

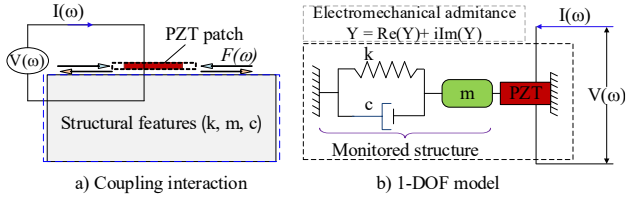

Figure 1. *Interaction between PZT sensor and structure [13, 37]*

2.2. Damage index using impedance signals

To detect structural damage, various statistical metrics are commonly employed for damage quantification. Sun et al. [14] introduced a statistical method based on the RMSD of impedance signatures. Subsequently, Raju [38] proposed the use of the correlation coefficient (CC) to assess signal similarity. Furthermore, Zagrai and Giurgiutiu [39] conducted a comprehensive evaluation of multiple statistical classification techniques for damage detection, including RMSD, mean absolute percentage deviation (MAPD), covariance change, and correlation coefficient deviation (CCD).

Among these statistical metrics, the RMSD index is most commonly adopted in studies for quantifying damage in concrete structures, owing to its high sensitivity to structural changes and damage progression [24, 31]. Therefore, in this study, the RMSD index is employed. It quantifies the variation between impedance signals and is calculated as follows:

$$RMSD(Z, Z^*) = \sqrt{\frac{\sum_{i=1}^{N}[Z^*(\omega_i) - Z(\omega_i)]^2}{\sum_{i=1}^{N}[Z(\omega_i)]^2}} \quad (2)$$

where $Z(\omega_i)$ and $Z^*(\omega_i)$ are the real parts of impedance signals measured before and after the damage occurrence at i^{th} frequency point, respectively, and N denotes the number of frequency sampling points in the sweep.

3. CSA-based compressive stress monitoring using numerical impedance signals

3.1. Capsule-like smart aggregate sensor

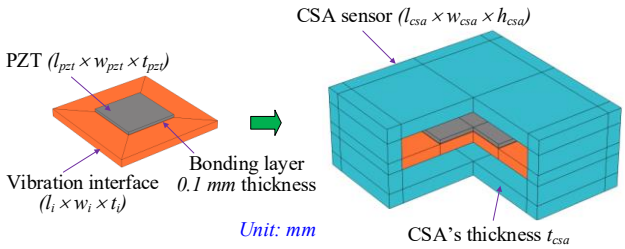

Figure 2. *Prototype of CSA sensor*

Figure 2 illustrates a general prototype of a CSA sensor. A PZT patch, with dimensions of $length \times width \times thickness = l_{pzt} \times w_{pzt} \times t_{pzt}$, is bonded to a vibration interface of size $(l_i \times w_i \times t_i)$ using a thin bonding layer. This PZT-interface assembly is installed at the center of a hollow encapsulation box, forming the complete CSA

sensor with overall dimensions of $(l_{csa} \times w_{csa} \times t_{csa})$. Detailed specifications and fabrication methods of the CSA components are described in the study by Pham et al. [30].

3.2. Finite element model of concrete cylinder embedded CSA under compression

Figure 3 illustrates a three-quarter view of the FE model of a concrete cylinder installed with the CSA. The CSA (thickness 2 mm) consists of a PZT-5A patch $(10 \times 10 \times 0.51\ mm)$, an interface $(21 \times 21 \times 1.5\ mm)$, and a hollow box $(25 \times 25 \times 11\ mm)$. Assuming that the PZT is perfectly mounted to the interface by using an adhesive layer [32] with a thickness of 0.1 mm, as reported in previous studies [24, 32]. The effect of the adhesive layer (i.e., thickness, degradation [40, 41]) has not been considered in the numerical model.

Aluminum material is used for the interface and the box. The CSA is placed at the center of the concrete specimen (with a diameter of $\phi_{cy} = 100\ mm$ and a height of $h_{cy} = 200\ mm$). As part of a preliminary study on the feasibility of CSA-based impedance monitoring, the EMI responses of the CSA are recorded under a sequence of applied axial compressive stresses S [31, 35]. The material properties of the concrete cylinder and the CSA's components are presented in Tables 1 and 2. The compressive strength of the concrete $(\sigma_c = 25.38\ MPa)$ was determined through uniaxial compression tests on three standard concrete specimens (100 × 200 mm) after 28 days of curing. For the impedance analysis, both the concrete and the CSA components are assumed to behave as linear elastic materials, following the approach in [24].

Table 1. *Material properties of PZT-5A*

Parameters	Symbol	Value	Unit
Young's modulus	E	62.1	GPa
Mass density	ρ	7750	kg/m^3
Poisson's ratio	ν	0.35	-
Damping loss factor	η	0.0125	-
Dielectric loss factor	δ	0.015	-
Dielectric constant	$\hat{\varepsilon}_{33}^{T}$	1.53×10^{-8}	Farad/m
Coupling constant	d_{31}	-1.71×10^{-10}	m/V

Table 2. *Material properties of concrete, aluminum, and bonding layer*

Parameters	Concrete	Aluminum	Bonding layer
Young's modulus, E (GPa)	25.47	70	5
Poisson's ratio, ν	0.20	0.33	0.38
Mass density, ρ (kg/m^3)	2400	2700	1700
Compressive strength, σ_c (MPa)	25.38	-	-

The FE model was carefully meshed to balance computational efficiency and numerical accuracy. A trial-and-error approach was employed to determine an appropriate element size, based on the observed differences in stress variation under applied compressive stresses. This method ensured that the selected mesh minimized numerical artifacts while maintaining reasonable computational cost. As shown in Figure 3, three-dimensional (3D) elements are modeled for the concrete cylinder and the CSA. The FE model has 15690 elements, including 14930 for the concrete cylinder and 760 elements for the CSA. The CSA meshing has 100, 100, 140, and 420 elements for the PZT, the bonding layer, the interface, and the aluminum box, respectively. Quadratic hexahedral elements are used for the CSA's components. Quadratic tetrahedral elements are used for the concrete domain. Axial compressive stresses S are applied to the top surface of the concrete cylinder as a uniform pressure, gradually increasing in increments to simulate loading stages. The bottom surface of the concrete cylinder is fully constrained in all directions (fixed support). Contact conditions between the PZT, interface, and aluminum encapsulation are modeled as perfectly bonded to simplify initial analysis. At this stage, the interfacial slip between layers is not considered. This assumption will be examined in future studies using cohesive contact elements or frictional interfaces to evaluate potential debonding effects.

To evaluate the feasibility of the CSA sensor, the applied stresses are designed to ensure the linear characteristic of the concrete material under compression [42, 43]. The compressive behavior of concrete is characterized by its stress-strain relationship. This relationship is linear when the stress is between $(0\sigma_c)$ and $(0.4\sigma_c)$, and becomes nonlinear as the stress increases from $(0.4\sigma_c)$ up to σ_c [43]. In this study, six loading scenarios (applied stresses S_1-S_6) [35] are simulated on the CSA-cylinder to obtain impedance signals. The compressive stresses are increasingly applied in a series from S_1 = 0 MPa $(0\sigma_c)$ to S_6 = 10.15 MPa $(0.4\sigma_c)$ with an interval of 2.03 MPa $(0.08\sigma_c)$.

To conduct the impedance analysis, a harmonic voltage of 1 V is applied to the top surface of the PZT patch, while the bottom surface is grounded to serve as the reference electrode. The impedance signatures of the CSA sensor are initially examined over a frequency range of 5-95 kHz, using 901 frequency sampling points, under the no-load condition S_1, to identify the sensitive frequency band. Once identified, this selected frequency range is used to analyze the variations in impedance responses under the subsequent applied compressive stress levels.

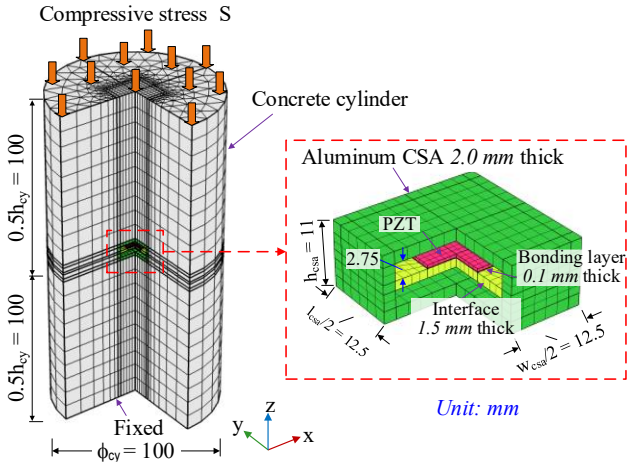

Figure 3. *FE model of CSA-concrete cylinder under stresses*

3.3. Compressive stress monitoring using numerical impedance features

Figure 4 presents the impedance response of the CSA sensor in the frequency band of 5-95 kHz under no applied stress (S_1 = 0 MPa). It can be observed that there is only one impedance resonant frequency peak at 25.3 kHz. The highest peak is contained in the frequency range of 20-30 kHz. It is well established that specific frequency ranges in the impedance spectrum capture the most significant structural information [31, 44, 45]. Therefore, the frequency range of 20-30 kHz (801 points) is selected to investigate the changes in impedance signals under compression. In the real-world application, impedance signals of CSA sensors will be monitored by using impedance analyzers (e.g., HIOKI 3532 or Agilent 4294A) with very fast responses, and the time for measuring will be in a very short period. In this way, the impedance signals of CSAs under compression are less likely to be influenced by ambient conditions. Noise-free impedance responses of CSA sensors under varying compressive loads have been demonstrated in the study by Ta et al. [35].

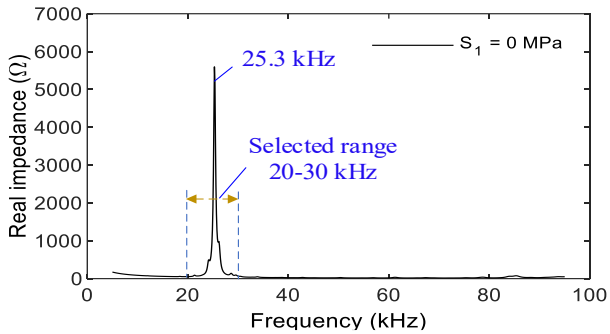

Figure 4. *Impedance signal of CSA in frequency range 5-95 kHz*

Figure 5 presents the changes in the impedance spectra of the CSA sensor under various axial compressive stresses ranging from 0 MPa (S_1) to 10.15 MPa (S_6) in the selected range (i.e., 20-30 kHz). As the compressive stress increases, the impedance signals exhibit a rightward shift, indicating the sensitivity of the CSA sensor to stress changes.

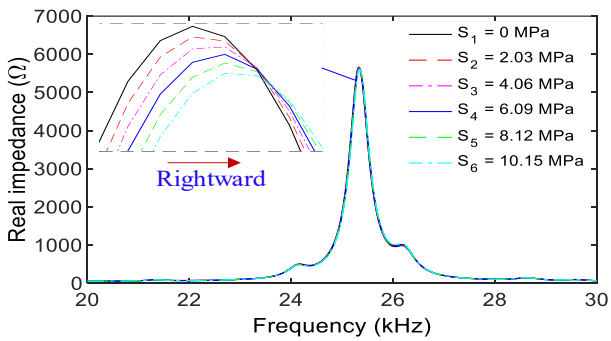

Figure 5. *Impedance signal of CSA in frequency range 20-30 kHz under compressive stresses*

Figure 6 illustrates the shift in the resonant frequency peak of the CSA sensor's impedance signal under increasing axial compressive stress. The resonant frequency remains constant between the initial loading stages, S_1 (0 MPa) and S_2 (2.03 MPa). A slight upward shift is observed from 25.325 kHz to 25.338 kHz between S_2 (2.03 MPa) and S_3 (4.06 MPa). Beyond this point, from S_3 to S_6 (4.06 MPa to 10.15 MPa), the resonant frequency stabilizes, showing no significant variation. This trend suggests a slight sensitivity of the frequency of the peak of the CSA sensor to axial compressive stress.

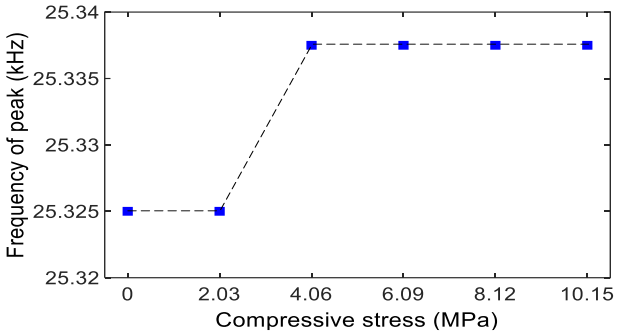

Figure 6. *Frequency of peak of CSAs under compressive stresses*

Figure 7 shows the variation in the magnitude of the peak frequency of the CSA sensor's impedance signal under increasing axial compressive stress. As the stress increases from S_1 (0 MPa) to S_6 (10.15 MPa), the peak magnitude gradually decreases from approximately 5665 Ω to 5605 Ω. This downward trend demonstrates the sensitivity of the impedance amplitude to axial compressive stress and suggests that the peak magnitude can serve as a potential indicator for estimating the compressive stress.

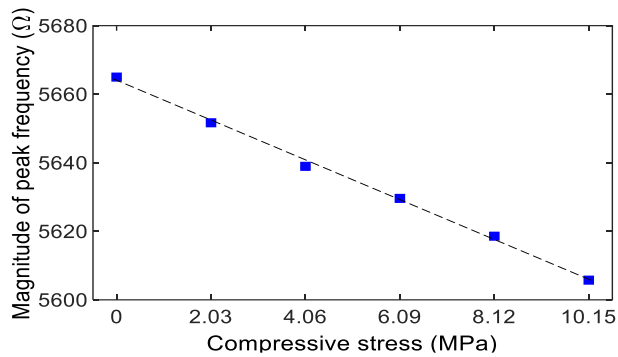

Figure 7. *Magnitude of peak frequency of CSAs under compressive stresses*

Figure 8 shows the RMSD indices, which are quantified from the impedance signals in the range (20-30 kHz). The RMSD magnitudes are gradually increased under stress variations. The progressive increase in RMSD values (from 0% to 4.54%) confirms the CSA sensor's sensitivity to stress-induced changes in the host concrete, indicating its capability for early-stage damage or stress monitoring.

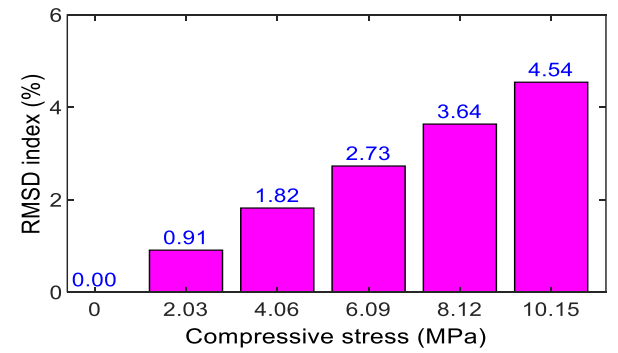

Figure 8. *RMSD indices of CSAs under compressive stresses*

3.4. Discussion and limitations

The numerical results of this study demonstrate that the CSA sensor exhibits clear sensitivity to axial compressive stress when embedded in a concrete cylinder. Both the shift in resonant frequency and the reduction in impedance amplitude confirm a strong correlation between the applied load and the sensor's electromechanical response. Notably, the RMSD index shows a progressive increase with increasing stress, reinforcing the CSA sensor's ability to detect stress-induced changes within the host structure.

In the current model, the CSA sensor is centrally embedded within the concrete specimen. The transition from concrete to aluminum, along with the change in cross-sectional geometry at the concrete-CSA interface, leads to localized stress concentrations at the sensor boundary. These stress concentrations may influence the impedance signals and will be systematically investigated in future studies. To better capture these effects, the application of the Concrete Damaged Plasticity (CDP) model [31] is proposed. This nonlinear constitutive model can account for material heterogeneity, boundary effects, and damage evolution under uniaxial compression, offering a more realistic simulation of concrete behavior under stress.

Furthermore, environmental influences such as temperature variation, humidity, and aging can significantly impact both the mechanical characteristics of concrete and the electromechanical behavior of the PZT-based CSA sensor [41, 46]. While these factors are not explicitly modeled in this initial study, future work will incorporate them. For instance, moisture effects can be simulated by adjusting concrete stiffness and damping properties, as well as the dielectric and piezoelectric constants of the PZT material.

It is also recognized that actual concrete structures are subject to complex loading conditions, including eccentric compression, bending, shear, and combined stress states. These can generate non-uniform stress fields, induce cracking, and alter the sensor-structure interaction in ways that significantly affect the impedance response. Accordingly, future extensions of this research will include simulations under such realistic loading scenarios to more thoroughly evaluate the CSA sensor's performance and reliability under practical conditions.

Moreover, although the present study focused on resonant frequency shifts and impedance amplitude changes, other spectral features such as peak broadening or attenuation were not explored in detail. These characteristics, however, may provide valuable insights into energy dissipation, material damping, and microstructural changes in concrete. In future work, a deeper spectral analysis will be conducted, including the evaluation of peak width or attenuation to better understand the interaction between the CSA sensor and the surrounding concrete matrix. This would enhance the interpretation of impedance signals beyond simplified scalar indices like RMSD or peak magnitude.

4. Conclusion

This study presented the numerical investigation into the use of the capsule-like smart aggregate (CSA) sensor for impedance-based stress monitoring in concrete structures. The detailed finite element model of the CSA-embedded concrete cylinder was developed to simulate the sensor's electromechanical response under applied compressive stress. Some findings are as follows:

- The CSA sensor shows detectable variations in impedance signatures under different compressive stress levels, confirming its stress sensitivity.

- The resonant frequency shift is insignificant while the impedance amplitude exhibits monotonic trends across the full loading range (up to 10.15 MPa), highlighting its effectiveness for stress detection.

- The RMSD index proves effective in quantifying impedance changes and is a reliable metric for identifying stress-induced variations.

The results support the feasibility of using CSA sensors for localized stress monitoring in concrete structures. Future work will focus on incorporating nonlinear material behavior, environmental influences, and complex loading conditions to improve model accuracy. In addition, a more comprehensive spectral analysis will be conducted to extract deeper diagnostic features from impedance data. These enhancements will enable broader and more reliable applications of CSA-based systems in real-world structural health monitoring (SHM).

REFERENCES

[1] N. Delatte, *Failure, distress and repair of concrete structures*. Elsevier, 2009.

[2] M. Alexander, and H. Beushausen, "Durability, service life prediction, and modelling for reinforced concrete structures - review and critique", *Cement and Concrete Research*, vol. 122, pp. 17-29, 2019.

[3] S. Taheri, "A review on five key sensors for monitoring of concrete structures", *Construction and Building Materials*, vol. 204, pp. 492-509, 2019.

[4] R. Rodrigues, S. Gaboreau, J. Gance, I. Ignatiadis, and S Betelu, "Reinforced concrete structures: A review of corrosion mechanisms and advances in electrical methods for corrosion monitoring", *Construction and Building Materials*, vol. 269, 121240, 2021.

[5] P.C. Chang, A. Flatau, and S.C. Liu, "Review paper: health monitoring of civil infrastructure", *Structural Health Monitoring*, vol. 2, no. 3, pp. 257-267, 2016.

[6] W. Fan, and P. Qiao, "Vibration-based damage identification methods: a review and comparative study", *Structural Health Monitoring*, vol. 10, no. 1, pp. 83-111, 2010.

[7] E.P. Carden, and P. Fanning, "Vibration based condition monitoring: a review", *Structural Health Monitoring,* vol. 3, no. 4, pp. 355-377, 2016.

[8] G. Park, H. Sohn, C.R. Farrar, and D.J. Inman, "Overview of piezoelectric impedance-based health monitoring and path forward", *Shock and Vibration Digest,* vol. 35, no. 6, pp. 451-463, 2003.

[9] V.G.M. Annamdas, and M.A. Radhika, "Electromechanical impedance of piezoelectric transducers for monitoring metallic and non-metallic structures: A review of wired, wireless and energy-harvesting methods", *Journal of Intelligent Material Systems and Structures,* vol. 24, no. 9, pp. 1021-1042, 2013.

[10] W. S. Na, and J. Baek, "A review of the piezoelectric electromechanical impedance based structural health monitoring technique for engineering structures", *Sensors,* vol. 18, no. 5, 1307, 2018.

[11] Y. Chen, and X. Xue, "Advances in the structural health monitoring of bridges using piezoelectric transducers", *Sensors*, vol. 18, no. 12, 4312, 2018.

[12] X. Fan, J. Li, and H. Hao, "Review of piezoelectric impedance based structural health monitoring: Physics-based and data-driven methods", *Advances in Structural Engineering*, vol. 24, no. 16, pp. 3609-3626, 2021.

[13] C. Liang, F.P. Sun, and C.A. Rogers, "Coupled electro-mechanical analysis of adaptive material systems-determination of the actuator power consumption and system energy transfer", *Journal of Intelligent Material Systems and Structures*, vol. 5, no. 1, pp. 12-20, 1994.

[14] F.P. Sun, Z. Chaudhry, C. Liang,, and C.A. Rogers, "Truss structure integrity identification using PZT sensor-actuator", *Journal of Intelligent Material Systems and Structures*, vol. 6, no. 1, pp. 134-139, 1995.

[15] G. Park, H.H. Cudney, and D.J. Inman, "Impedance-based health monitoring of civil structural components*", Journal of Infrastructure Systems,* vol. 6, no. 4, pp. 153-160, 2000.

[16] V. Giurgiutiu, A. Reynolds, and C.A. Rogers, "Experimental investigation of E/M impedance health monitoring for spot-welded structural joints", *Journal of Intelligent Material Systems and Structures*, vol. 10, no. 10, pp. 802-812, 1999.

[17] S. Bhalla, A.S.K. Naidu, C.W. Ong, C.K. Soh, "Practical issues in the implementation of electromechanical impedance technique for NDE", *in Smart structures, devices, and systems, SPIE*, vol. 4935, pp. 484-494, 2002.

[18] Z. Chaudhry, F. Lalande, A. Ganino, C. Rogers, and J. Chung, "Monitoring the integrity of composite patch structural repair via piezoelectric actuators/sensors", *in Proc. 36th Structures, Structural Dynamics and Materials Conference, USA*, 1995.

[19] G. Park, H. H. Cudney, and D. J. Inman, "Feasibility of using impedance-based damage assessment for pipeline structures", *Earthquake Engineering & Structural Dynamics,* vol. 30, no. 10, pp. 1463-1474, 2001.

[20] H. Zhu, H. Luo, D. Ai, and C. Wang, "Mechanical impedance-based technique for steel structural corrosion damage detection", *Measurement*, vol. 88, pp. 353-359, 2016.

[21] N. Kaur, S. Goyal, K. Anand, and G. K. Sahu, "A cost-effective approach for assessment of pre-stressing force in bridges using piezoelectric transducers", *Measurement*, vol. 168, 108324, 2021.

[22] C. K. Soh, K. K. H. Tseng, S. Bhalla, and A. Gupta, "Performance of smart piezoceramic patches in health monitoring of a RC bridge", *Smart Materials and Structures,* vol. 9, no. 4, pp. 533-542, 2000.

[23] S. Park, S. Ahmad, C. B. Yun, and Y. Roh, "Multiple crack detection of concrete structures using impedance-based structural health monitoring techniques", *Experimental Mechanics*, vol. 46, no. 5, pp. 609-618, 2006.

[24] D. Ai, H. Luo, and H. Zhu, "Numerical and experimental investigation of flexural performance on pre-stressed concrete structures using electromechanical admittance", *Mechanical Systems and Signal Processing,* vol. 128, pp. 244-265, 2019.

[25] T. C. Huynh, and J. T. Kim, "Quantitative damage identification in tendon anchorage via PZT interface based impedance monitoring technique", *Smart Structures and Systems*, vol. 20, no. 2, pp. 181-195, 2017.

[26] N. L. Dang, Q. Q . Pham, and J. T. Kim, "Piezoelectric-based hoop-type interface for impedance monitoring of local strand breakage in prestressed multi-strand anchorage", *Structural Control and Health Monitoring,* vol. 28, no. 1, e2649, 2020.

[27] H. Gu, G. Song, H. Dhonde, Y. L. Mo, and S. Yan, "Concrete early-age strength monitoring using embedded piezoelectric transducers", *Smart Materials and Structures*, vol. 15, no. 6, pp. 1837-1845, 2006.

[28] Q. Kong, S. Fan, X. Bai, Y. L. Mo, and G. Song, "A novel embeddable spherical smart aggregate for structural health monitoring: part I. Fabrication and electrical characterization", *Smart Materials and Structures*, vol. 26, no. 9, 095050, 2017.

[29] D. Wang, H. Song, and H. Zhu, "Embedded 3D electromechanical impedance model for strength monitoring of concrete using a PZT transducer", *Smart Materials and Structures*, vol. 23, no. 11, 115019, 2014.

[30] Q.Q. Pham, Q.B. Ta, and J.T. Kim, "Capsule-like smart aggregate with pre-determined frequency range for impedance-based stress monitoring", *Sensors*, vol. 23, no. 1, 434, 2022.

[31] S. Zhao, S. Fan, J. Yang, and S. Kitipornchai, "Numerical and experimental investigation of electro-mechanical impedance based concrete quantitative damage assessment", *Smart Materials and Structures,* vol. 29, no. 5, 055025, 2020.

[32] T. C. Huynh, N. L. Dang, and J. T. Kim, "Preload monitoring in bolted connection using piezoelectric-based smart interface", *Sensors*, vol. 18, no. 9, 2766, 2018.

[33] K. D. Nguyen, and J. T. Kim, "Smart PZT-interface for wireless impedance-based prestress-loss monitoring in tendon-anchorage connection", *Smart Structures and Systems,* vol. 9, no. 6, pp. 489-504, 2012.

[34] N. L. Dang, Q. Q. Pham, and J. T. Kim, "Hybrid vibration-impedance monitoring in prestressed concrete structure with local strand breakage", *Smart Structures and Systems*, vol. 30, no. 5, pp. 463-477, 2022.

[35] Q. B. Ta, Q. Q. Pham, N. L. Pham, and J. T. Kim, "Integrating the Capsule-like Smart Aggregate-Based EMI Technique with Deep Learning for Stress Assessment in Concrete", *Sensors*, vol. 24, no. 14, 2024, 4738.

[36] T. T. Nguyen, J. T. Kim, Q. B. Ta, D. D. Ho, T. T. V. Phan, and T. C. Huynh, "Deep learning-based functional assessment of piezoelectric-based smart interface under various degradations", *Smart Structures and Systems*, vol. 28, no. 1, pp. 69-87, 2021.

[37] C. Liang, F. Sun, and C. A. Rogers, "Electro-mechanical impedance modeling of active material systems", *Smart Materials and Structure*s, vol. 5, no. 2, pp. 171-186, 1996.

[38] V. Raju, "*Implementing impedance-based health monitoring technique*", Master's Thesis, Virginia Polytechnic Institute State University, Blacksburg, VA, 1998.

[39] A.N. Zagrai, and V. Giurgiutiu, "Electro-mechanical impedance method for crack detection in thin plates*", Journal of Intelligent Material Systems Structures*, vol. 12, no. 10, pp. 709-718, 2001.

[40] T. C. Huynh, T. D. Nguyen, D. D. Ho, N. L. Dang, and J. T. Kim, "Sensor fault diagnosis for impedance monitoring using a piezoelectric-based smart interface technique", *Sensors*, vol. 20, no. 2, 510, 2020.

[41] D. Ai, C. Lin, and H. Zhu, "Embedded piezoelectric transducers based early-age hydration monitoring of cement concrete added with accelerator/retarder admixtures", *Journal of Intelligent Material Systems and Structures*, vol. 32, no. 8, pp. 847-866, 2021.

[42] P. D. Simão, H. Barros, C. C. Ferreira, and T. Marques, "Closed-form moment-curvature relations for reinforced concrete cross sections under bending moment and axial force", *Engineering Structures*, vol. 129, pp. 67-80, 2016.

[43] H. L. Minh, S. Khatir, M. A. Wahab, and T. Cuong-Le, "A concrete damage plasticity model for predicting the effects of compressive high-strength concrete under static and dynamic loads", *Journal of Building Engineering*, vol. 44, 103239, 2021.

[44] N. L. Dang, T. C. Huynh, and J. T. Kim, "Local strand-breakage detection in multi-strand anchorage system using an impedance-based stress monitoring method-feasibility study", *Sensors*, vol. 19, no. 5, 1054, 2019.

[45] Y. Yang, Y. Hu, and Y. Lu, "Sensitivity of PZT impedance sensors for damage detection of concrete structures", *Sensors,* vol. 8, no.1, pp. 327-346, 2008.

[46] T. C. Huynh, N. L. Dang, and J. T. Kim, "PCA-based filtering of temperature effect on impedance monitoring in prestressed tendon anchorage", *Smart Structures and Systems*, vol. 22, no. 1, pp. 57-70, 2018.